Japanese Journal of Applied Physics

The Japan Society of Applied Physics

REGULAR PAPER • OPEN ACCESS

High-mobility 4 μm MOVPE-grown (100) β-Ga_2O_3 film by parasitic particles suppression

To cite this article: Ta-Shun Chou *et al* 2023 *Jpn. J. Appl. Phys.* **62** SF1004

View the article online for updates and enhancements.

You may also like

- Perturbation analysis of second-order nonlinearity and its effectiveness for radiofrequency bulk acoustic wave devices
Masanori Ueda, Toshio Nishizawa, Shinji Taniguchi et al.
- Statistical modeling of V_{th} distribution in ovonic threshold switches based on physical switching models
Shinji Yokogawa
- Power device breakdown mechanism and characterization: review and perspective
Ruizhe Zhang and Yuhao Zhang

This content was downloaded from IP address 89.245.22.228 on 21/03/2023 at 08:36

OPEN ACCESS

Japanese Journal of Applied Physics 62, SF1004 (2023) REGULAR PAPER
https://doi.org/10.35848/1347-4065/acb360

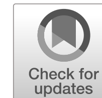

High-mobility 4 μm MOVPE-grown (100) β-Ga_2O_3 film by parasitic particles suppression

Ta-Shun Chou[1*], Palvan Seyidov[1], Saud Bin Anooz[1], Raimund Grüneberg[1], Jana Rehm[1], Thi Thuy Vi Tran[1], Andreas Fiedler[1], Kornelius Tetzner[2], Zbigniew Galazka[1], Martin Albrecht[1], and Andreas Popp[1]

[1]Leibniz-Institut für Kristallzüchtung (IKZ), Max-Born-Str. 2, D-12489 Berlin, Germany
[2]Ferdinand-Braun-Institut, Leibniz-Institut für Höchstfrequenztechnik, Gustav-Kirchhoff-Straße 4, D-12489 Berlin, Germany

*E-mail: ta-shun.chou@ikz-berlin.de

Received November 29, 2022; revised January 5, 2023; accepted January 15, 2023; published online February 9, 2023

In this work, we comprehensively investigate the development of unwanted parasitic particles in the MOVPE chamber while growing μm level films. The density of the parasitic particles is found to be pronounced at film thicknesses starting from >1.5 to 2 μm. These particles seem to induce structural defects such as twin lamellae, thereby harming the electrical properties of the grown film. The origin of the parasitic particle is attributed to the parasitic reactions within the chamber triggered by the promoted gas-phase reactions during the growth process, which can be largely reduced by increasing the total gas flow and decreasing the showerhead distance to the susceptor. A film thickness of up to 4 μm has been achieved after minimizing the density of parasitic particles. Thereby, RT Hall measurements reveal carrier mobilities of 160 $cm^2V^{-1}s^{-1}$ at carrier concentrations of 5.7 × 10^{16} cm^{-3}. © 2023 The Author(s). Published on behalf of The Japan Society of Applied Physics by IOP Publishing Ltd

Supplementary material for this article is available online

1. Introduction

Beta-gallium oxide (β-Ga_2O_3) is a promising compound semiconductor material with great potential for high-power electronic application[1,2] owing to its ultrawide bandgap of up to 4.9 eV[3,4] and a theoretical breakdown field of up to 8 MV cm^{-1}.[5] With such a high breakdown field, β-Ga_2O_3-based power devices are expected to outperform other developed semiconductor materials such as silicon carbide (SiC) and gallium nitride (GaN).[2] In addition to the excellent properties of β-Ga_2O_3, the availability of a low-cost single-crystal substrate of β-Ga_2O_3 has been demonstrated using various growth techniques, such as Czochralski (Cz),[6,7] vertical Bridgeman (VB),[8,9] and edge-defined film-fed growth (EFG),[10] which allows possible mass wafer production and the development of the high-quality homoepitaxial film.

The investigation of homoepitaxial β-Ga2O3 film has been reported by different deposition methods, including molecular beam epitaxy,[11–14] metalorganic vapor-phase epitaxy (MOVPE),[15–20] halide vapor-phase epitaxy (HVPE),[21,22] and low-pressure chemical vapor deposition.[23,24] Among the above methods, the MOVPE technique is the preferred growth method for industrial applications due to its advantages of a high growth rate and the capability for mass production. The electron concentration of homoepitaxial β-Ga_2O_3 film can be achieved wide range from low-10^{16} cm^3 to mid-10^{19} cm^3 using Sn[25] and Si[26] as n-type dopants.

With the above merits, β-Ga_2O_3-based power devices have been widely developed in lateral structure[27–29] and also in vertical structure.[30] To effectively exploit the high theoretical breakdown field of β-Ga_2O_3, vertical device structure has attracted great interest recently since the peak electric field is buried in the bulk to avoid the surface states-induced device failure. Moreover, the breakdown voltage of vertical metal–oxide–semiconductor field-effect transistors can be scaled up by thickening the drift layer, resulting in a higher blocking voltage without increasing chip area. Therefore, the development strategy can be summarized as continuously increasing the thin-film thickness while maintaining good electrical properties.

However, we recently found parasitic particles formed on the MOVPE-grown film surface as a killer defect, which significantly deteriorates carrier mobility by inducing structural defects. Such parasitic particles can be observed easily using conventional light microscopy and are more pronounced in films grown above 1.5 μm film thickness. In this study, we determined the formation condition of parasitic particles in the MOVPE chamber while growing μm-level films. The mechanism of the parasitic particle formation and the solutions are proposed and discussed, and a great improvement in electrical properties is observed after minimizing the density of parasitic particles.

2. Experimental methods

β-Ga_2O_3 films with nominal thicknesses up to 4.0 μm were grown using MOVPE on (100) oriented β-Ga_2O_3 substrates with an offcut of 4° towards [00$\bar{1}$]. The MOVPE used in this work consists of a vertical showerhead low-pressure and cold-wall chamber (Structured Materials Industries, Inc. -USA). The distance between the showerhead and substrate susceptor of the MOVPE system is adjustable between 8 cm to 1 cm, and the closest distance presented in the current work is 1.5 cm. High-quality Mg-doped β-Ga_2O_3 single crystals for (100) oriented substrates were grown by the Czochralski method at Leibniz-Institut für Kristallzüchtung (IKZ).[31,32] CrysTec GmbH Berlin provided Wafering and polishing services to prepare 10 × 10 mm^2 substrates. After removing the damaged layer due to polishing by etching in phosphoric acid (H_3PO_4, 85%) for 15 min, the substrates were then annealed in an oxygen atmosphere at 900 °C for 60 min to pronounce the terraced structure on the substrate surface.[33] The growth temperature was fixed at 800 °C. The chamber pressure was kept at 25 mbar. Triethylgallium (TEGa), high-purity oxygen gas (5 N), and

Content from this work may be used under the terms of the Creative Commons Attribution 4.0 license. Any further distribution of this work must maintain attribution to the author(s) and the title of the work, journal citation and DOI.
© 2023 The Author(s). Published on behalf of The Japan Society of Applied Physics by IOP Publishing Ltd

tetraethylorthosilicate (TEOS) were used as gallium precursors, oxidant, and Si dopant, respectively. High-purity Ar (5 N) acted as push (carrier) gas and mixing gas (precursor mixing in the showerhead), and the supplied amount of Ar push gas was kept at 500 sccm, and Ar uniform gas was varied between 1800 sccm and 4000 sccm. The oxygen flow was varied between 320 sccm and 480 sccm, the TEGa molar flow was tuned accordingly from 60 sccm to 90 sccm to maintain the desired O_2/Ga ratio, and the resulting growth rate was between 0.6 and 0.9 μm h^{-1}. The detailed experimental results of the current growth condition are referred to in Refs. 18, 34. The surface morphology of the grown β-Ga_2O_3 films was investigated by atomic force microscopy (AFM) (Bruker Dimension Icon, USA). The electrical data were obtained by conductivity and Hall effect measurements at room temperature in the van-der-Pauw configuration using small InGa eutectic contacts exhibiting ohmic behavior. The chemical concentration of the incorporated Si dopant and the thickness were determined by the secondary ion mass spectrometry (SIMS) performed by RTG Mikroanalyse GmbH Berlin. The composition of the parasitic particle was identified with energy-dispersive X-ray spectroscopy (EDX) using the electron beam of SEM as an excitation source.

3. Results and discussion

Representative images of parasitic particles formed during β-Ga_2O_3 MOVPE growth conditions are taken by conventional light microscopy, as shown in Fig. 1, respectively. The particles are initially found pronounced at a thickness above 1.5 μm with a showerhead distance of 8 cm under the condition addressed in our previous work,[18] appearing as black dots on the film surface [Fig. 1(a)]. However, regardless of the film thickness, the size of particles is usually in the range of 1–3 μm in terms of diameter [Fig. 1(b)] with a random sphere-like shape. It is also found that the appearance of particles is independent of the growth rate (Fig. 2) but depends on the film thickness, and the density of particles increases with the film thickness, as shown in Fig. 3.

It is interesting to note that the growth rate of such particles is much higher than the growth rate for planar films (0.6–0.9 μm h^{-1}) since the particles usually start forming after ~1.5 μm film thickness with a size of μm-level. Therefore, it is possible that once particles have nucleated, the size of the particle increases through a chemical vapor deposition (CVD) process. The growth kinetics of small spherical particles has been applied previously to explain the formation of nanoparticles in MOVPE-grown AlGaInN,[35] and the steady state radial growth rate (*dr*/*dt*) is given by Eq. (1):[36]

$$dr/dt = D \cdot v \cdot (C_b - C_s)/[r + D/k], \quad (1)$$

where r is the particle radius, D is the diffusion coefficient, C_b is the bulk molar concentration of precursor within the ambient, C_s is the molar concentration of precursor at the particle surface, k is the surface reaction rate, which is assumed to be independent of the particle size, and v is the molar volume of the particle. It should also be noted that possible reactant depletion effects are ignored in this mechanism, and the surface reaction rate is assumed to be the product of the mean molecular velocity υ, and the reactive sticking coefficient s.

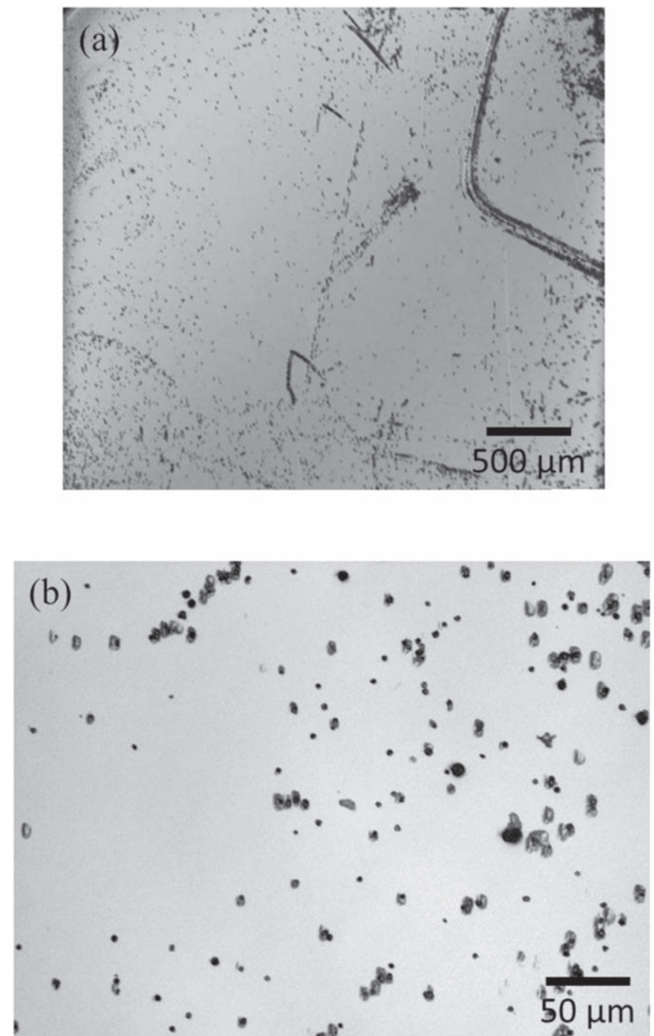

Fig. 1. (a) Light microscopy image of the parasitic particles on the grown film surface and (b) a zoom-in image of the parasitic particles.

Considering the small size limit, $r \ll D/k$, the radial growth rate can be reduced to Eq. (2), which is simply the kinetic limit controlled by the surface reaction, and the concentration of precursor can be approximated to be C_b. The radial growth rate from Eq. (2) can be as high as 10^2–10^3 nm s^{-1} for the current growth conditions (see supporting information)

$$dr/dt \approx (\upsilon \cdot s) \cdot v \cdot C_b, \text{ when } r \ll D/k. \quad (2)$$

This mechanism suggests that the parasitic particle may grow as large as ~1 μm in diameter within 1–2 s, indicating that the particle CVD growth mechanism can experimentally generate the size range observed above. With the CVD growth mechanism, the thickness-dependent particle density shown in Fig. 3 can also be interpreted from Eq. (2) that the accumulation of unreacted Ga precursor in the chamber is increasing along the growth process, promotes the nucleation and the growth of the parasitic particles. Different from the case of AlN,[37] particle formation does not influence film growth in terms of growth rate. The growth rate of β-Ga_2O_3

© 2023 The Author(s). Published on behalf of The Japan Society of Applied Physics by IOP Publishing Ltd

Fig. 2. A comparison of light microscopy images of the films (both 3 μm thick) grown with different growth rates by scaling the O_2/Ga ratio while keeping other growth parameters fixed as well as the showerhead distance at 8 cm: (a) 0.75 μm h^{-1} and (b) 3.0 μm h^{-1}.

film is stable over time regardless of the thickness as determined by the SIMS measurements (Fig. 4), indicating that the adducts of the parasitic reaction are not directly from the precursors involved in the film growth but the accumulated precursors in the chamber.

The embedded particles in the grown film generally induce harmful structural defects, as shown in Fig. 5 (red circles). The induced structural defects have a long axis perpendicular to the [001] direction, which is similar to the twin lamellae reported previously.[38] One can also observe that some particles are on the top of the surface, and some are located within the center of induced defects, indicating the time dependency of particle formation. Since the particle density increases with the film thickness, the carrier mobility of layers above 3 μm is measurable only with $n > 6 \times 10^{17}$ cm^{-3}. However, the measured mobilities are lower than the record values[39] at similar doping levels and thinner thicknesses, as indicated in Fig. 6. For $n < 6 \times 10^{17}$ cm^{-3}, the layers are still conductive, but a reliable measurement of the Hall effect is not possible, which is ascribed to a sudden drop in electron mobility with decreasing electron concentration (mobility collapse). A similar mobility collapse below a critical carrier concentration is observed in GaN and is explained by a high density of dislocations forming walls of potential barriers for electron transport.[38,40] For the layer

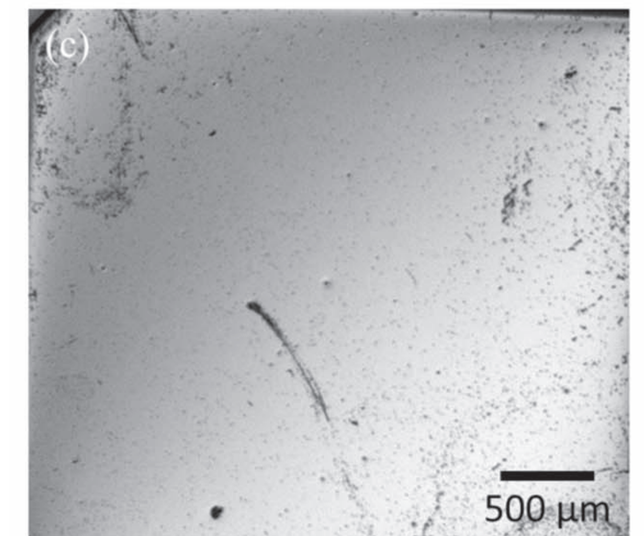

Fig. 3. A comparison of light microscopy images of the films grown with different thicknesses while keeping other growth parameters fixed as well as the showerhead distance at 8 cm: (a) 2.0 μm, (b) 3.0 μm and (c) 4.0 μm.

© 2023 The Author(s). Published on behalf of The Japan Society of Applied Physics by IOP Publishing Ltd

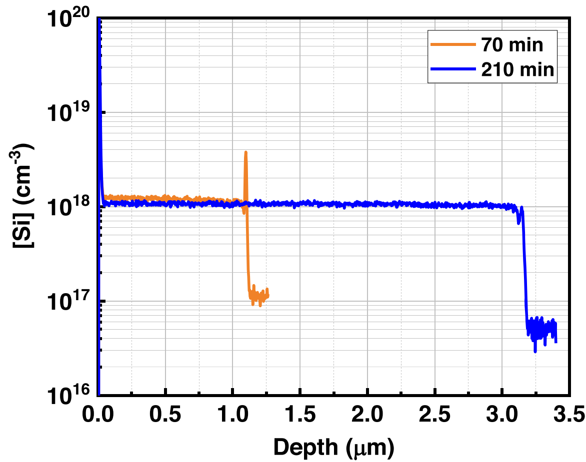

Fig. 4. (Color online) A comparison of SIMS measurement of the films grown with different growth times while keeping other growth parameters fixed with a showerhead distance of 8 cm: 70 min (1 μm) and 210 min (3 μm).

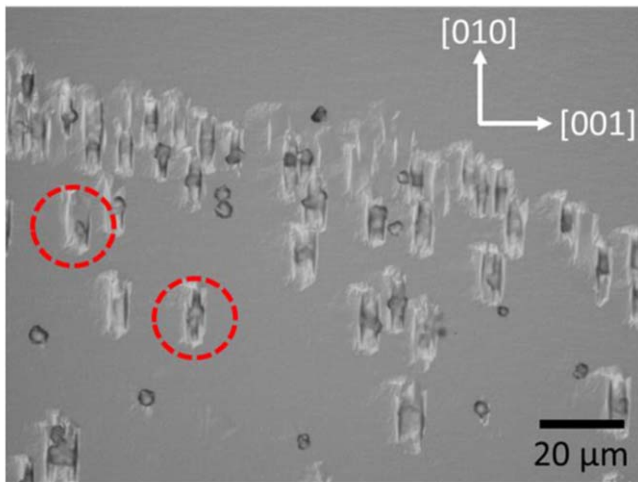

Fig. 5. (Color online) Zoom-in light microscopy image of the parasitic particles and the induced defects.

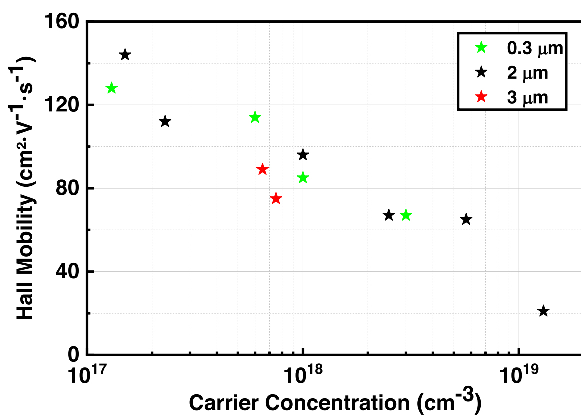

Fig. 6. (Color online) Carrier Hall mobility as a function of the carrier Hall concentration at 300 K for β-Ga_2O_3 homoepitaxially grown by MOVPE on (100)-oriented substrates (black asterisk: 2 μm, red asterisk: 3 μm, and green asterisk: 0.3 μm) from the growth condition (showerhead distance is 8 cm) addressed in Ref. 18 (2 μm and 3 μm) and Ref. 19 (0.3 μm), respectively.

thickness of 2 μm, the carrier mobility is comparable with the recorded values in the range from 10^{17} to $10^{19}\,cm^{-3}$, as reported previously;[18] however, not available for the regime below $10^{17}\,cm^{-3}$.

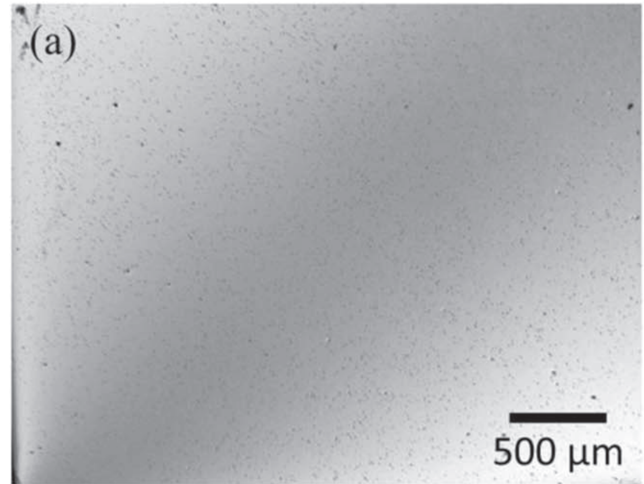

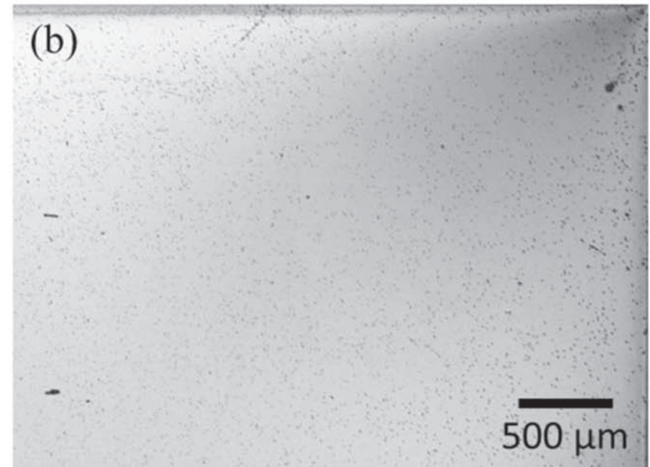

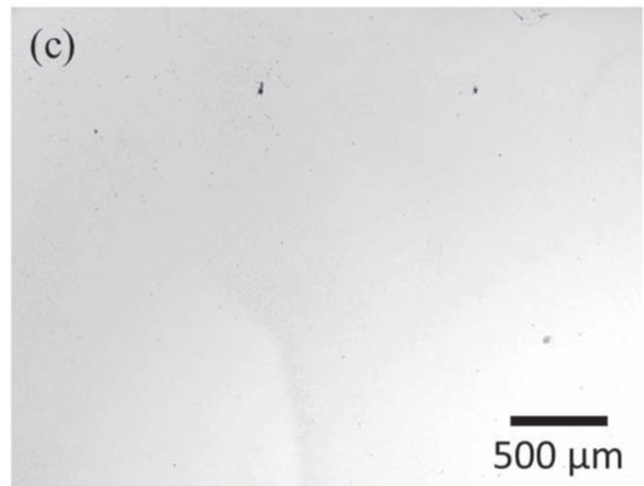

Fig. 7. A comparison of light microscopy images of the films grown up to 3 μm with different showerhead distances while keeping other growth parameters fixed: (a) 8 cm, (b) 4 cm and (c) 1.5 cm.

The particles are either randomly distributed or follow certain trajectories, such as straight lines or curve lines, suggesting that the gas flow carries the particles, and the distribution of the particles partially reflects the streamlining of gas flow on the growing surface. A detailed thermodynamic analysis under similar growth conditions as this work has been performed by Goto et al.[41] The analysis revealed that the only thermodynamically-stable solid product is the

© 2023 The Author(s). Published on behalf of The Japan Society of Applied Physics by IOP Publishing Ltd

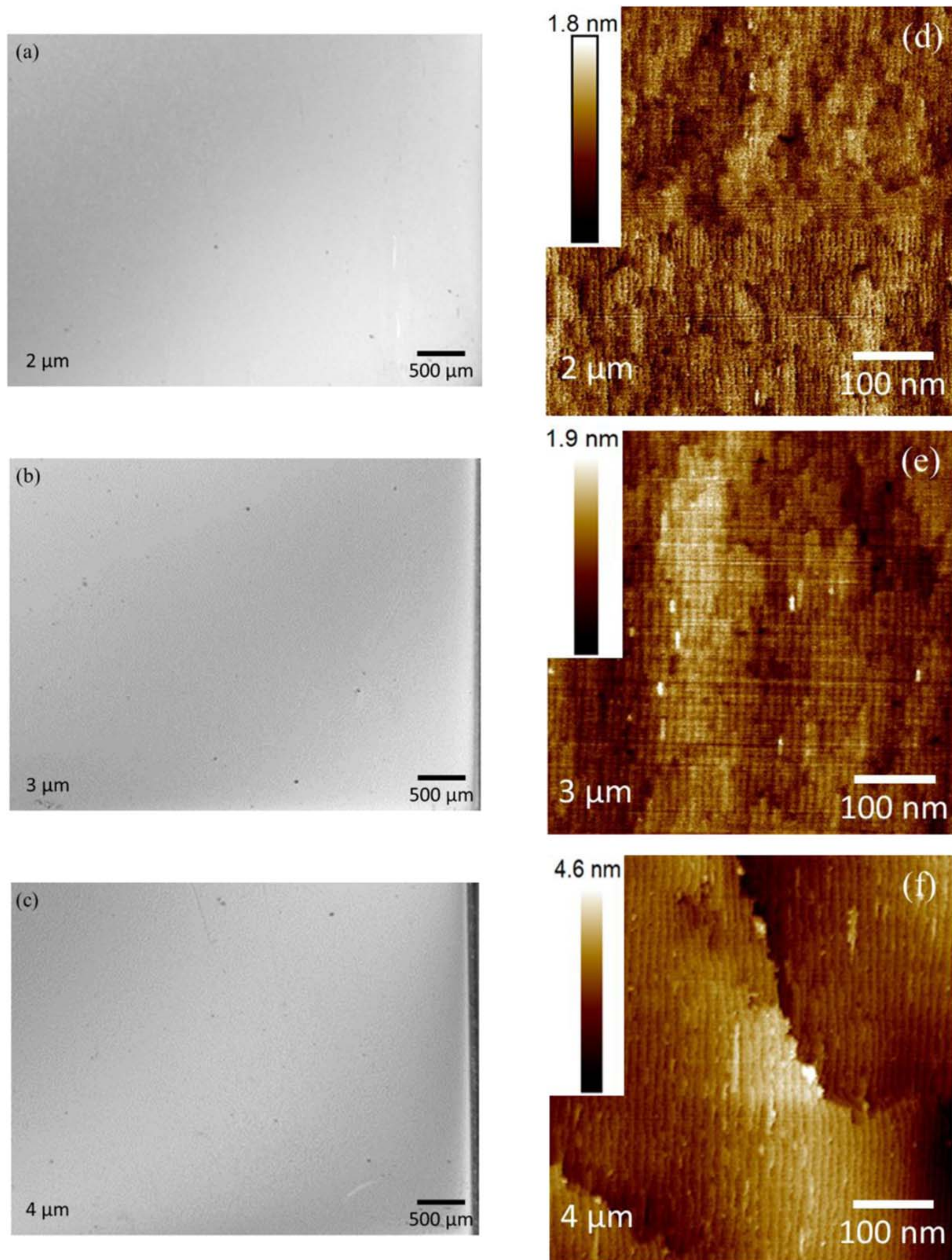

Fig. 8. (Color online) Light microscopy images of the films grown with a mixing gas flow of 4000 sccm and a showerhead distance at 1.5 cm: (a) 2 μm, (b) 3 μm and (c) 4 μm. The corresponding AFM images of the film with thicknesses: (d) 2 μm, (e) 3 μm and (f) 4 μm.

β-Ga_2O_3. Other possible species, like Ga_2O and GaO, are volatile. Therefore, one can conclude that the observed parasitic particle is actually β-Ga_2O_3 in the particle shape formed from the gaseous phase reactions in the chamber and is formed in the same growth condition as the growth of β-Ga_2O_3 films. Local EDX measurements have been performed (not shown here) at the particle-free area and directly on the particles. As expected, the two measurements (free area and particles) show similar signal intensity for Ga and O, which clearly proves that there is no significant difference in the components of the particles and the grown film. With the known composition and the possible CVD mechanism of the parasitic particles, two strategies are considered to eliminate them: (1) decreasing the residence time of the precursors before being transported to the boundary layer of the film surface and (2) avoiding the nucleation of parasitic particles. The former can be realized by shortening the showerhead distance to the susceptor, and the latter can be carried out by

© 2023 The Author(s). Published on behalf of The Japan Society of Applied Physics by IOP Publishing Ltd

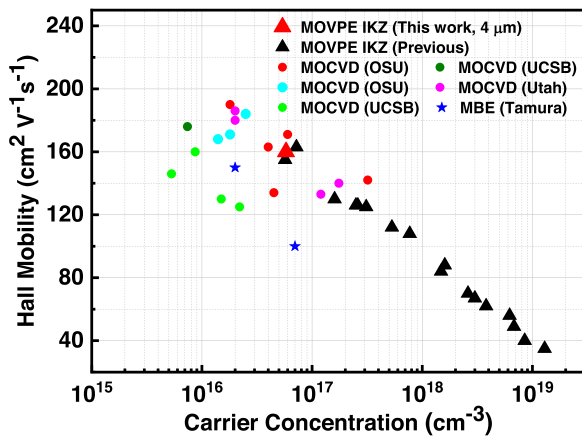

Fig. 9. (Color online) The electron Hall mobility in 4 μm (160 $cm^2 V^{-1} s^{-1}$) β-Ga_2O_3 films grown on (100) β-Ga_2O_3 substrate (showerhead distance at 1.5 cm) as a function of carrier concentration (red closed triangles). Black closed triangles represent the mobility in the films from our previous work,[18,19,34,44] including the previous record values of 2.2 μm (155 $cm^2 V^{-1} s^{-1}$) and 3 μm (163 $cm^2 V^{-1} s^{-1}$). Other symbols show results from the literature of different substrate orientations and various film thicknesses: ● (∼ 3 μm),[16] ● (1.25 μm),[20] ● (2.5–3.2 μm),[17] ● (3.2 μm)[15] ● (0.4–1 μm)[45] and ★ (0.7 μm).[11]

diluting the chamber with a higher total gas flow to avoid reaching the critical concentration for the nucleation of the parasitic particles.

The influence of the showerhead distance on the growth of (100) β-Ga_2O_3 films was first investigated. It is found that while keeping all other growth parameters constant, the growth rate nearly doubles by decreasing the showerhead distance from 8 to 1.5 cm. Since the current condition is mass transport-limited, the thin-film growth rate was limited by the amount of Ga precursors transported to the boundary layer. The observed increment of growth rate at a lower showerhead distance suggests that more Ga precursors transport into the boundary layer without being consumed by the parasitic reactions (as the source of particle formation) during the transportation, and the input Ga precursor gas flow rate into the showerhead is the same while decreasing the showerhead distance. A comparison of the samples grown up to 3 μm under different showerhead distances is shown in Figs. 7(a)–7(c). The density of the parasitic particles is reduced significantly at a lower showerhead distance (1.5 cm) compared with a higher showerhead distance (4 cm and 8 cm) while fixing all other growth parameters and growing the same film thickness.

By keeping the showerhead distance at 1.5 cm, the influence of total gas flow on the particle density was studied. In the current system, there are two major gas (Ar) sources that contribute to the total gas flow rate in the MOVPE system: (1) the mixing gas flow in the showerhead and (2) the precursor carrier gas flow. The former is supplied by additional tubes directly connected to the sidewall of the showerhead, which is functional as mixing all precursors before being carried to the growing surface; the latter carries the mixed precursors from the showerhead to the growing surface. Even though the two gas sources both contribute to the total gas flow, the resulting influences on the growth process are very different. The change of the mixing gas flow has a minor impact on the thin-film growth rate but is important to the thickness homogeneity of the grown film. On the other hand, the thin-film growth rate is very sensitive to the carrier gas flow rate; as previously reported,[42] a slight change in quantity might largely increase or reduce the growth rate. One can conclude that the carrier gas determines the transportation of the precursor, and the mixing gas flow has more impact on the distribution of precursors in the chamber.

Since our purpose is to suppress particle formation without disturbing the growth dynamics, tuning the mixing gas flow rate is preferred to homogenize the local concentration of precursors in the chamber. A lower density of particles is observed by increasing the mixing gas flow rates from 1800 sccm to the range between 3000 sccm and 4000 sccm. To ensure the necessary thickness homogeneity of the grown film as well as the O_2/Ga ratio, the TEGa flow rate and the oxygen flow rate are increased to 90 sccm and 480 sccm, respectively. Combining a showerhead distance of 1.5 cm and a higher total gas flow rate, (100) β-Ga_2O_3 films, up to 4 μm, with a low embedded particle density while maintaining a desired step-flow morphology, has been successfully demonstrated, as shown in Fig. 8. A similar approach of increasing the total gas flow rate has also been reported by HVPE-grown β-Ga_2O_3 films[43] to reduce the parasitic particles, and suggested that the gaseous reaction is more likely to occur under a lower total gas flow rate. Previously, we have reported[34] that the films exhibited good electrical properties with a reduced particle density at the thicknesses of 2 μm and 3 μm. With further development addressed in this work, the room temperature Hall mobility approaches a maximum value of 160 $cm^2 \cdot V^{-1} \cdot s^{-1}$ at an electron concentration of about 5.7×10^{16} cm^{-3} at 4 μm thickness. This electron mobility value is the first reported electron mobility for a 4 μm thick MOVPE-grown β-Ga_2O_3 film and is compared with state-of-the-art values from the literature and our previous work in Fig. 9.

4. Conclusions

In conclusion, parasitic particles are one of the killer defects in MOVPE β-Ga_2O_3 films while growing above several μm-level thicknesses. As indicated by light microscopy and SEM characterization, particles are in the size of 1–3 μm, which matches the estimation of the CVD growth mechanism. These particles and induced defects result in a mobility collapse of thick layers above 2 μm. Process optimization is implemented by lowering the showerhead position and increasing the total gas flow rate during the growth. A film thickness of up to 4 μm has been successfully demonstrated with carrier mobilities of up to 160 $cm^2 V^{-1} s^{-1}$ measured at room temperature.

Acknowledgments

The authors would like to thank Dr. Thomas Straubinger for reading the manuscript. This work was performed in the framework of GraFOx, a Leibniz ScienceCampus. The work was funded by the BMBF under grant number 16ES1084K, the European Community (Europäische Fonds für regionale Entwicklung- EFRE) under grant number 1.8/15, and by the

© 2023 The Author(s). Published on behalf of The Japan Society of Applied Physics by IOP Publishing Ltd

Deutsche Forschungsgemeinschaft under project funding reference number PO-2659/1-2.

ORCID iDs

Ta-Shun Chou https://orcid.org/0000-0002-3897-6573
Kornelius Tetzner https://orcid.org/0000-0001-6720-8138

1) K. Sasaki, M. Higashiwaki, A. Kuramata, T. Masui, and S. Yamakoshi, J. Cryst. Growth **378**, 591 (2013).
2) M. Higashiwaki and G. H. Jessen, Appl. Phys. Lett. **112**, 060401 (2018).
3) Z. Galazka, Semicond. Sci. Technol. **33**, 113001 (2018).
4) H. Peelaers and C. G. Van de Walle, Phys. Status Solidi b **252**, 828 (2015).
5) S. Ghose, S. Rahman, L. Hong, J. S. Rojas-Ramirez, H. Jin, K. Park, R. Klie, R. Droopad, J. S. Rojas-Ramirez, and H. Jin, J. Appl. Phys. **122**, 095302 (2017).
6) Z. Galazka et al., Appl. Phys. Lett. **120**, 152101 (2022).
7) Z. Galazka, J. Appl. Phys. **131**, 031103 (2022).
8) K. Hoshikawa, T. Kobayashi, and E. Ohba, J. Cryst. Growth **546**, 125778 (2020).
9) E. Ohba, T. Kobayashi, T. Taishi, and K. Hoshikawa, J. Cryst. Growth **556**, 125990 (2021).
10) A. Kuramata, K. Koshi, S. Watanabe, Y. Yamaoka, T. Masui, and S. Yamakoshi, Jpn. J. Appl. Phys. **55**, 1202A2 (2016).
11) K. Sasaki, A. Kuramata, T. Masui, E. G. Víllora, K. Shimamura, and S. Yamakoshi, Appl. Phys. Express **5**, 035502 (2012).
12) P. Mazzolini, P. Vogt, R. Schewski, C. Wouters, M. Albrecht, and O. Bierwagen, APL Mater. **7**, 022511 (2019).
13) P. Vogt and O. Bierwagen, Appl. Phys. Lett. **108**, 072101 (2016).
14) H. Okumura, M. Kita, K. Sasaki, A. Kuramata, M. Higashiwaki, and J. S. Speck, Appl. Phys. Express **7**, 095501 (2014).
15) Y. Zhang, F. Alema, A. Mauze, O. S. Koksaldi, R. Miller, A. Osinsky, and J. S. Speck, APL Mater. **7**, 022506 (2019).
16) L. Meng, Z. Feng, A. F. M. A. U. Bhuiyan, and H. Zhao, Cryst. Growth Des. **22**, 3896 (2022).
17) F. Alema, Y. Zhang, A. Osinsky, N. Valente, A. Mauze, T. Itoh, and J. S. Speck, APL Mater. **7**, 121110 (2019).
18) T.-S. Chou, P. Seyidov, S. Bin Anooz, R. Grüneberg, T. Thi Thuy Vi, K. Irmscher, M. Albrecht, Z. Galazka, J. Schwarzkopf, and A. Popp, AIP Adv. **11**, 115323 (2021).
19) S. Bin Anooz et al., J. Phys. D: Appl. Phys. **54**, 034003 (2021).
20) Z. Feng, A. F. M. Anhar Uddin Bhuiyan, M. R. Karim, and H. Zhao, Appl. Phys. Lett. **114**, 250601 (2019).
21) K. Goto, H. Nakahata, H. Murakami, and Y. Kumagai, Appl. Phys. Lett. **117**, 222101 (2020).
22) H. Murakami et al., Appl. Phys. Express **8**, 015503 (2015).
23) Z. Feng, M. R. Karim, and H. Zhao, APL Mater. **7**, 02514 (2019).
24) S. Rafique, L. Han, S. Mou, and H. Zhao, Opt. Mater. Express **7**, 3561 (2017).
25) M. Baldini, M. Albrecht, A. Fiedler, K. Irmscher, R. Schewski, and G. Wagner, ECS J. Solid State Sci. Technol. **6**, Q3040 (2017).
26) T.-S. Chou et al., Appl. Phys. Lett. **121**, 032103 (2022).
27) K. Tetzner, O. Hilt, A. Popp, S. Bin Anooz, and J. Würfl, Microelectron. Reliab. **114**, 113951 (2020).
28) M. H. Wong, K. Sasaki, A. Kuramata, S. Yamakoshi, and M. Higashiwaki, Jpn. J. Appl. Phys. **55**, 1202B9 (2016).
29) M. Higashiwaki, K. Sasaki, A. Kuramata, T. Masui, and S. Yamakoshi, Appl. Phys. Lett. **100**, 013504 (2012).
30) M. H. Wong, K. Goto, Y. Morikawa, A. Kuramata, S. Yamakoshi, H. Murakami, Y. Kumagai, and M. Higashiwaki, Appl. Phys. Express **11**, 064120 (2018).
31) Z. Galazka et al., J. Cryst. Growth **404**, 184 (2014).
32) Z. Galazka, R. Uecker, D. Klimm, K. Irmscher, M. Naumann, M. Pietsch, A. Kwasniewski, R. Bertram, S. Ganschow, and M. Bickermann, ECS J. Solid State Sci. Technol. **6**, Q3007 (2017).
33) S. Ohira, N. Arai, T. Oshima, and S. Fujita, Appl. Surf. Sci. **254**, 7838 (2008).
34) T.-S. Chou et al., submitted to Appl. Phys. Lett.
35) J. R. Creighton, G. T. Wang, W. G. Breiland, and M. E. Coltrin, J. Cryst. Growth **261**, 204 (2004).
36) N. T. K. Thanh, N. Maclean, and S. Mahiddine, Chem. Rev. **114**, 7610 (2014).
37) Y. Feng, H. Wei, S. Yang, Z. Chen, L. Wang, S. Kong, G. Zhao, and X. Liu, Sci Rep. **3**, 6416 (2014).
38) A. Fiedler, R. Schewski, M. Baldini, Z. Galazka, G. Wagner, M. Albrecht, and K. Irmscher, J. Appl. Phys. **122**, 165701 (2017).
39) S. Bin Anooz et al., Appl. Phys. Lett. **116**, 182106 (2020).
40) D. C. Look and J. R. Sizelove, Phys. Rev. Lett. **82**, 1237 (1999).
41) K. Goto, K. Ikenaga, N. Tanaka, M. Ishikawa, H. Machida, and Y. Kumagai, Jpn. J. Appl. Phys. **60**, 045505 (2021).
42) T.-S. Chou, S. Bin Anooz, R. Grüneberg, D. Natascha, W. Miller, T. T. V. Tran, J. Rehm, and A. Popp, J. Cryst. Growth **592**, 126737 (2022).
43) S. Sdoeung, K. Sasaki, S. Masuya, K. Kawasaki, J. Hirabayashi, A. Kuramata, and M. Kasu, Appl. Phys. Lett. **118**, 172106 (2021).
44) R. Schewski et al., APL Mater. **7**, 022515 (2019).
45) A. Bhattacharyya, P. Ranga, S. Roy, J. Ogle, L. Whittaker-Brooks, and S. Krishnamoorthy, Appl. Phys. Lett. **117**, 142102 (2020).

© 2023 The Author(s). Published on behalf of The Japan Society of Applied Physics by IOP Publishing Ltd